Journal of Applied Physics ARTICLE scitation.org/journal/jap

Optically thick GaInAs/GaAsP strain-balanced quantum-well tandem solar cells with 29.2% efficiency under the AM0 space spectrum

Cite as: J. Appl. Phys. **132**, 184502 (2022); doi: 10.1063/5.0125998
Submitted: 14 September 2022 · Accepted: 20 October 2022 ·
Published Online: 8 November 2022

View Online

Export Citation

CrossMark

Ryan M. France,[1,a)] Jennifer Selvidge,[1,2] Kunal Mukherjee,[3] and Myles A. Steiner[1]

AFFILIATIONS

[1]National Renewable Energy Laboratory, Golden, Colorado 80401, USA
[2]Materials Department, University of California, Santa Barbara, Santa Barbara, California 93106, USA
[3]Department of Material Science and Engineering, Stanford University, Stanford, California 94305, USA

[a)]**Author to whom correspondence should be addressed:** ryan.france@nrel.gov

ABSTRACT

GaAs is often used as a multijunction subcell due to its high material quality on GaAs substrates, despite having a non-optimal bandgap. The bandgap can be beneficially reduced using many layers of thin, strain-balanced GaInAs in a superlattice or quantum well device, but achieving excellent carrier collection without increased recombination has proven challenging. Here, we develop and demonstrate high performance, optically thick GaInAs/GaAsP strain-balanced solar cells. Excellent material quality is achieved in thick superlattices by using growth conditions that limit progressive thickness and composition fluctuations. Bandgap-voltage offsets as low as 0.31 V are shown in superlattice cells using thin, highly strained GaP barriers. Optically thick superlattice cells with over 2500 nm of total GaInAs in the depletion region are developed, enabling 3.8 mA/cm^2 of extra photocurrent beyond the GaAs band edge under the AM0 space spectrum. Optimized superlattice solar cells are incorporated into two-junction devices that achieve 29.2% efficiency under the AM0 space spectrum due to their improved bandgap combination and high subcell voltages.

© 2022 Author(s). All article content, except where otherwise noted, is licensed under a Creative Commons Attribution (CC BY) license (http://creativecommons.org/licenses/by/4.0/). https://doi.org/10.1063/5.0125998

INTRODUCTION

III–V solar cells achieve extremely high conversion efficiencies both by having very low non-radiative recombination and by utilizing multiple materials with a range of bandgaps that span the solar spectrum. While some bandgaps are accessed using materials that are lattice-matched to the host epitaxial substrate, other desirable materials are lattice-mismatched to the substrate and require metamorphic buffers, wafer bonding, or strained layers in order to be employed. Metamorphic buffers access lattice-mismatched material through the intentional introduction of dislocations to relieve mismatch strain, enabling thick but defected absorbing material.[1–3] Wafer bonding enables the integration of materials that were originally grown on two separate host substrates.[4–6] Finally, a succession of thin, strained layers can be coherently implemented without generating dislocations if the layers remain below the critical thickness for dislocation formation, termed strained-layer superlattice (SLS) solar cells or multiple quantum well (MQW) solar cells.[7–10]

MQW and SLS solar cells have been investigated for over two decades,[11–13] leading to a large body of both experimental and theoretical literature. Compressively strained GaInAs on GaAs substrates beneficially lowers the bandgap from 1.41 eV, the GaAs bandgap, to 1.34 eV, a more optimal bandgap for both single junction and multijunction solar cells. Using GaAs barriers, the net strain quickly accumulates and only a few QWs are possible.[14] Stress-balancing with tensile-strained GaAsP barriers allows many more QWs to be incorporated, increasing absorption.[7,15–17]

Multiple quantum well solar cells use GaAsP barriers that are thick enough so that there is no overlap of the electronic wavefunctions of adjacent GaInAs wells, thereby providing quantum confinement in one dimension. While quantum confinement aids absorption near the excitonic energy, it also increases the effective bandgap from that of the bulk GaInAs bandgap, and so partially negates some of the benefit of the low-bandgap GaInAs. Photogenerated carriers escape the well by thermionic emission

and recapture into the well is prevented by placing the MQWs in the depleted region of a p–i–n device where transport is dominated by carrier drift.[18] While the i-region leads to good carrier collection in a solar cell, it also leads to increased depletion region recombination, and so QW devices often have a high J_{02} diode component and a reduced fill factor.[10,19] Low background doping is needed so that the QW stack is fully depleted at the maximum power point, otherwise, the fill factor will further suffer.[20]

Strained-layer superlattice solar cells, on the other hand, utilize barriers that are thin enough to allow overlap between the wavefunctions of adjacent GaInAs wells. As has been suggested, thin barriers should enable tunneling transport between GaInAs wells and can be beneficial for carrier collection.[14,17,21] Figure 1 shows calculated carrier lifetimes in a single 8.5 nm $Ga_{0.894}In_{0.106}As$ quantum well as a function of GaAsP barrier thickness before either thermionic emission or tunneling occurs, using calculations described previously.[7,17,22] For this material combination, the carrier lifetimes of tunneling and thermionic emission are equivalent at about 5 nm, indicating that carrier transport shifts from thermionic emission to tunneling transport at barrier thicknesses below 5 nm. Increased wavefunction overlap may also have the benefit of reduced carrier confinement and, thus, a reduced bandgap. Thus, thin-barrier SLS solar cells have some advantages over QW solar cells in theory, but there are few high-quality device results.[15]

For both types of devices, large numbers of individual GaInAs wells are needed to significantly increase the absorption in the QW wavelength range, which presents multiple materials challenges. First, the entire GaInAs/GaAsP stack needs to be carefully stress-balanced to prevent plastic relaxation via dislocation formation; even a small error in the stress-balancing can easily exceed the critical thickness over the course of a thick stack.[23] Second, lateral thickness or composition modulation slowly onsets throughout a QW stack due to elastic relaxation or surface instability and must be limited.[24–27] Third, the many interfaces between GaInAs and GaAsP must not result in unintentional morphology, defects, or low bandgap material.[28] Until recently, only partially absorbing QW solar cells have been created due to limitations on the amount of GaInAs, and voltages are often low.[15] Applying a reflector behind the QW stack increases absorption by providing a second pass to incident light, reaching quantum efficiencies of 60%–80% in the sub-bandgap region,[15,29,30] though introducing a reflector can be challenging in a multijunction cell where sub-bandgap light also needs to be transmitted to an adjacent, lower bandgap junction.[31,32]

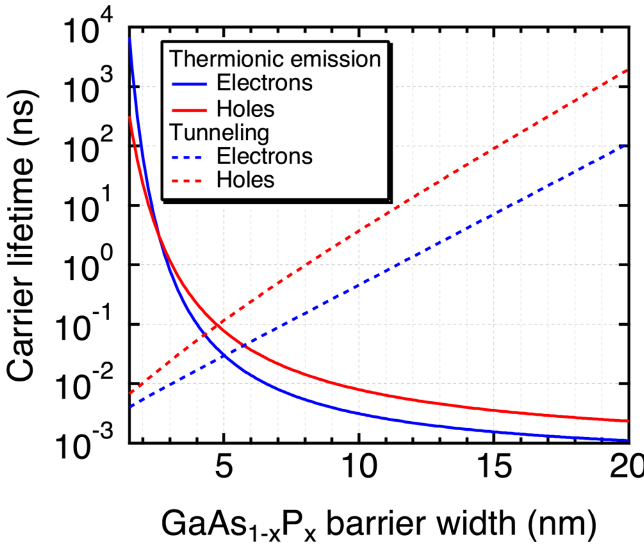

FIG. 1. Electron and hole tunneling and thermionic emission carrier lifetime in a single, 8.5 nm GaInAs quantum well, for variable GaAsP barrier thickness.

Recently, we demonstrated that 300 QWs can be incorporated into devices while maintaining excellent material quality, enabling high efficiency three-junction inverted metamorphic solar cells.[33] In this paper, we show the materials development of high quality GaInAs/GaAsP QWs and investigate very thin-barrier GaInAs/GaAsP solar cells to enhance absorption below the GaAs band edge. We vary the thickness of the GaAsP barrier while fixing the GaInAs thickness, maintaining stress-balancing by changing the GaAsP composition. In this way, the GaInAs fraction of the quantum-well stack increases, enabling additional absorption for a given i-region thickness. We reduce the barrier thickness to 2 nm so that carrier transport changes from strictly thermionic emission of a QW cell to a combination of thermionic emission and tunneling in an SLS cell. In thin-barriers solar cells, extra care is needed to control lateral thickness or composition modulation, which otherwise leads to major structural defects. With controlled modulation, we test the performance of thin-barrier GaInAs/GaAsP as the number of GaInAs layers increases and can implement over 2500 nm of total GaInAs without major performance loss, thus creating an optically thick structure. We also demonstrate QW solar cells using GaP barriers with a thickness of 2 nm, where GaInAs makes up 80% of the intrinsic region. Optimized SLS devices are incorporated into high performance two-junction solar cells that take advantage of the bandgap combination enabled by the SLS subcell.

EXPERIMENTAL METHODS

The solar cells in this study are rear-heterojunction solar cells [Fig. 2(a)], which were previously found to have better performance than both QW[34] and GaInP[35] front junction solar cells. Solar cells were grown by atmospheric pressure metalorganic vapor phase epitaxy (MOVPE) on (001) GaAs substrates miscut 2° toward (111) B, using trimethylindium, triethylgallium, trimethylgallium, trimethylaluminum, arsine, and phosphine precursors for the constituent atoms, and silane, dieththylzinc, carbon tetrachloride, and hydrogen selenide precursors for the dopants. Dimethylhydrazine was used as a nitrogen source in the front contact layer. Growth temperatures between 620 and 700 °C were used for all layers, with growth rates between 2 and 7 μm/h. Notably, the GaInAs/GaAsP layers were grown between 625 and 650 °C at 2.5–3.1 μm/h without stop-growths between layers. The growth direction was inverted, and the structure consisted of a GaInP stop-etch layer, followed by a GaInNAs:Se contact layer, a GaInP:Se window, 1 μm GaAs:Si emitter, 2 μm undoped GaInAs/GaAsP quantum well (QW) or

© Author(s) 2022

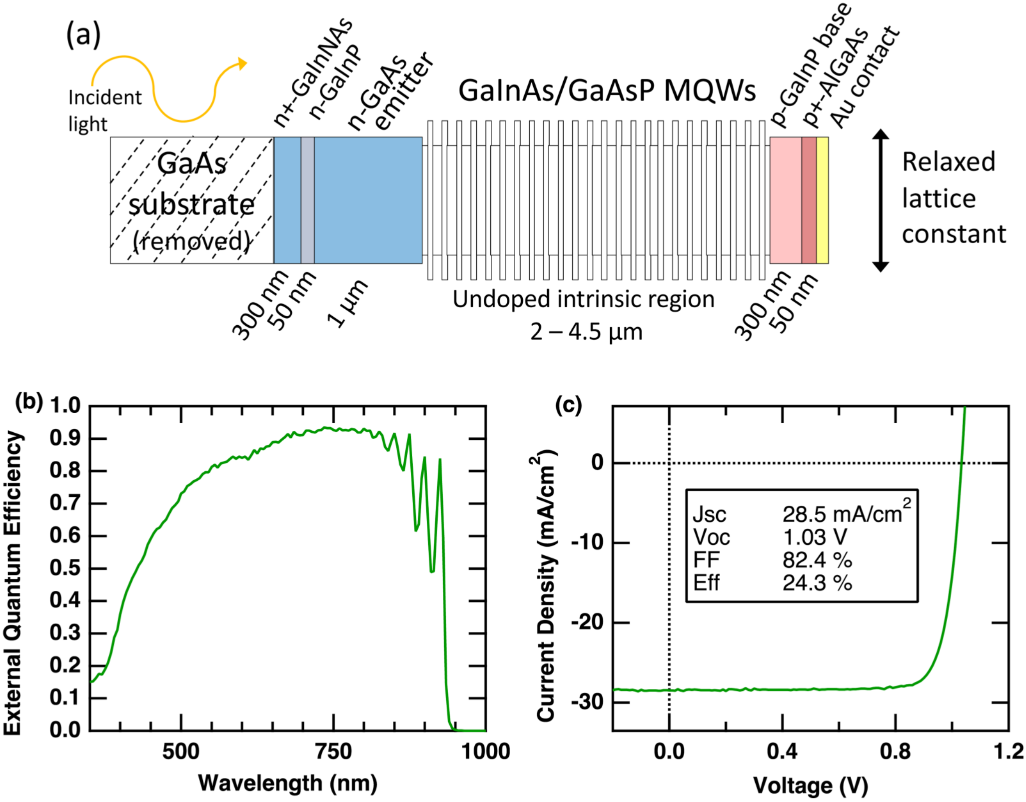

FIG. 2. (a) Illustration of the single junction test structure. The device is a rear-heterojunction cell with a thick GaAs emitter and stress-balanced GaInAs/GaAsP in the intrinsic region. The growth direction is from left to right. (b) External quantum efficiency and (c) J–V curve of the baseline structure, which is based off the structure in Ref. 8.

superlattice (SL) layers, 0.1 μm GaAs:Zn, 0.3 μm GaInP:Zn base, and GaAs:C contact layer. During growth, *in situ* wafer curvature was used to ensure proper stress balancing of the QW or SL layers, as described in Ref. 8.

After the growth, a planar Au contact was electrodeposited onto the GaAs:C back contact layer, and the samples were then inverted and bonded onto a silicon handle using epoxy.[36] Then, the GaAs substrate was removed by wet-chemical etching, front Ni/Au contacts were electroplated onto the GaInNAs:Se layer, the contact layer was removed between the grid fingers, and devices were mesa isolated using selective etchants. Finally, a MgF_2/ZnS anti-reflection coating was thermally deposited.

Quantum efficiency was measured on a custom-made tool using chopped, monochromatic light and a lock-in amplifier to measure extracted current, which was compared to a calibrated reference cell. For tandem devices, continuous light biasing was provided by 450 or 850 nm light emitting devices (LEDs), and luminescent coupling effects on the quantum efficiency were removed.[37] The quantum efficiency was used to establish the proper spectrum for illuminated J–V measurements on a continuous solar simulator equipped with LEDs to modify the spectrum of a Xe bulb. The light intensity was set using calibrated reference cells. Electroluminescence was measured with a fiber optic and spectral evolution spectroradiometer using the method described in Ref. 35, and dark JV subcell curves were calculated from the reciprocity theorem.[38] Independent measurement and certification of the tandem device were provided by the cell module and performance team at NREL.

AFM was measured using the tapping mode of a Veeco Dimension 3100 atomic force microscope (AFM), and the root mean squared (RMS) roughness was evaluated from an area of $50 \times 50\,\mu\text{m}^2$. Scanning transmission electron microscopy (STEM) images were collected using a ThermoFisher Talos G2 200X TEM/STEM using a standard bright field (BF) circular detector, standard annular dark field (ADF) detector, and standard high angle annular dark field (HAADF) detector. A 10.5 mrad beam convergence angle was used. The foils were prepared in a FEI Helios Dualbeam Nanolab 600 using standard lift out and thinning procedures.

The tunneling and thermionic emission carrier lifetimes in Fig. 1 were calculated using techniques described previously,[22]

$$\frac{1}{\tau_{tun}} = \frac{n\pi\hbar}{2t_w^2 m_w^*} e^{-\frac{2t_b}{\hbar}\sqrt{2m_b^* E_b}} \tag{1}$$

© Author(s) 2022

and

$$\frac{1}{\tau_{therm}} = \frac{1}{t_w}\sqrt{\frac{kT}{2\pi m_w^*}}e^{-\frac{E_b}{kT}}, \tag{2}$$

where t_w and t_b are the well and barrier thicknesses, m_w and m_b are the effective masses, and E_b is the barrier height from the energy level n, assumed to be the ground state $n = 1$. The calculation used a fixed $Ga_{0.894}In_{0.106}As$ composition and thickness and variable GaAsP thickness, where the composition was modified with the thickness to result in stress-balancing.[39]

DEVELOPMENT OF GROWTH CONDITIONS

Stress-balanced GaInAs/GaAsP quantum well solar cell designs using thick GaAsP barriers are discussed at length in Ref. 8. These QW cells show excellent external quantum efficiency and have power conversion efficiency of 27.2% under the AM1.5 global spectrum. The structure from Ref. 8 is adapted to this experiment by increasing the number of wells and using a GaInP window instead of AlInP for ease and reproducibility. There are 80 sets of 85 Å $Ga_{0.894}In_{0.106}As$ wells that are stress-balanced with 170 Å $GaAs_{0.902}P_{0.098}$ barriers. With 170 Å barriers, carrier transport is dominated by thermionic emission.[7,22] Figures 2(b) and 2(c) show the performance and structure of this baseline device. Other than the i-region, the cell structure is consistent throughout the experiments, and so the thick-barrier device provides a benchmark against which to compare solar cells with thinner barriers.

To develop thin-barrier solar cells, a variety of stress-balanced GaAsP/GaInAs layers were developed with different GaAsP barrier thickness and composition. In each case, the GaInAs composition and thickness are nominally fixed to $Ga_{0.894}In_{0.106}As$ and 85 Å, respectively, but the GaAsP composition and thickness are simultaneously adjusted to enable stress-balancing with thinner GaAsP layers.[39] Test structures with 30 GaInAs/GaAsP repeats were grown and characterized using wafer curvature and XRD to confirm appropriate stress-balancing. Then, solar cells devices were grown using the structure in Fig. 2 by implementing the GaInAs/GaAsP layers into the undoped i-region of the device. The total i-region thickness was kept at a constant 2 μm, by varying the number of GaInAs/GaAsP repeat units.

Even though properly stress-balanced, implementing thin, 3 nm, $GaAs_{0.5}P_{0.5}$ barriers resulted in poor device performance. Figures 3(a) and 3(b) show the QE and IV, respectively, of the initial thin-barrier device (red line), showing reduced performance. The surface of the solar cell is rough, shown in Fig. 4(a), and has an Rrms roughness of 11 nm.

The thickness of strained GaAsP required to stress-balance 85 Å of $Ga_{0.895}In_{0.105}As$ is less than the Matthews–Blakeslee critical thickness for all possible compositions of GaAsP,[39–41] even considering the impact of CuPt atomic ordering.[42] Therefore, standard dislocation nucleation and glide from strained two-dimensional growth are not expected. In addition, the surface does not have a crosshatched appearance, normally indicative of dislocation nucleation and glide. However, three-dimensional relaxation is possible, such as strain-relaxation through lateral composition or thickness modulation from the step-bunching of surface steps or the formation of quantum dots.[43] The combination of rough surface morphology and poor device performance is indicative of such elastic relaxation within the stress-balanced GaInAs/GaAsP stack.

The prior literature has shown that gradual lateral thickness modulation can progress during the growth of strained quantum wells, eventually resulting in the formation of defects. Previously, Sb surfactant was used to limit this relaxation, presumably by reducing indium migration.[44–46] Guidelines for limiting thickness modulation include utilizing high growth rates, high V/III ratio, low substrate miscut, and low temperature.[25] In this study, we investigate the impact of the GaInAs V/III ratio on device performance, with the intent of limiting indium migration and thus 3D elastic relaxation. No changes to the GaAsP layers were made.

Figure 3 shows the EQE and JV of solar cells with varied AsH_3 partial pressure during the growth of the GaInAs layers. Device performance of thin-barrier solar cells improves with increasing AsH_3 partial pressure, implying a benefit to the material quality from increased AsH_3 partial pressure. Final devices have a QE near 100% near 800 nm along with significant sub-bandgap

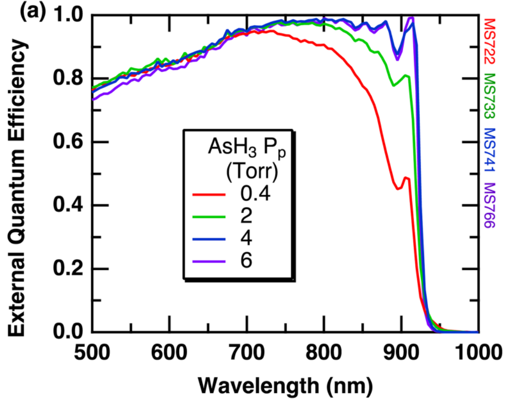

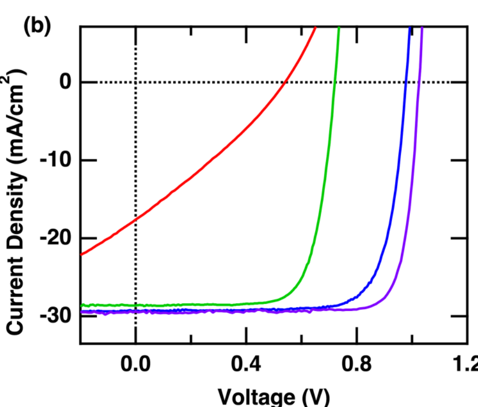

FIG. 3. (a) EQE and (b) JV of GaInAs/GaAsP solar cells with variable AsH_3 partial pressure in GaInAs layers.

© Author(s) 2022

absorption due to the amount of GaInAs in these thin-barrier SL devices. The open circuit voltage (Voc) of the best device is 1.02 V, and the Woc (=Eg/q − Voc) is 0.32 V, demonstrating that high material quality can be achieved.

Cross-sectional transmission electron microscopy is performed on the best and worst devices in this sample set to further investigate the cause of device degradation and impact of AsH_3 partial pressure, shown in Fig. 4. The initial layers of both samples are flat, with minimal roughness, and have thicknesses of 7.7 and 3.3 nm for the GaInAs and GaAsP layers, respectively, close to the nominal value from the growth rate calibration. Assuming uniform compositions of both GaAsP and $Ga_{0.895}In_{0.105}As$, the stress-balancing condition estimates that the GaAsP composition is $GaAs_{0.5}P_{0.5}$.

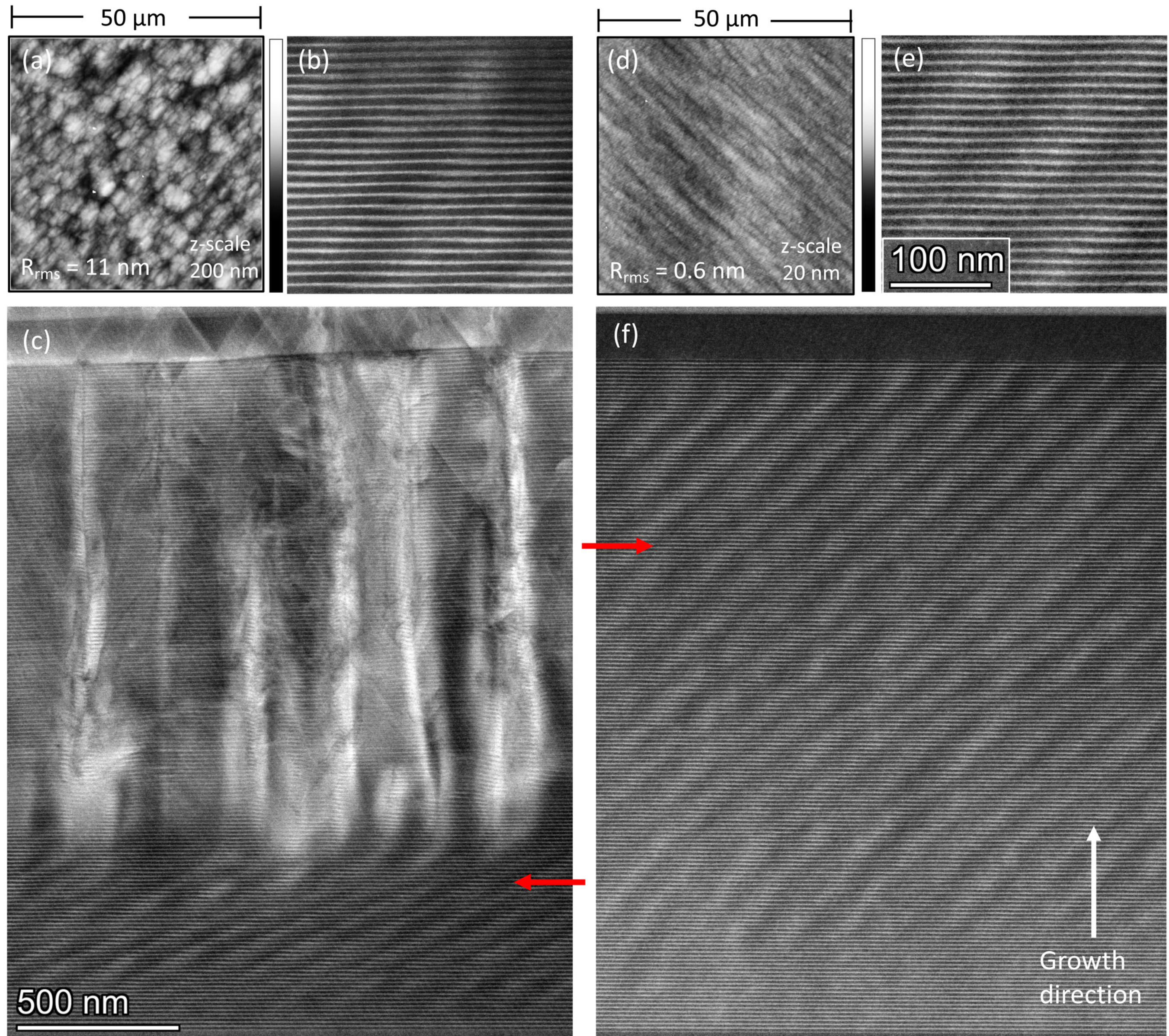

FIG. 4. (a) AFM of the surface of the GaInAs/GaAsP solar cell using low arsine overpressure in GaInAs layers. (b) High magnification and (c) low magnification cross-sectional STEM image of the same sample. (d)–(f) Similar images of the solar cell with high arsine overpressure in GaInAs layers. The red arrows on the low magnification images indicate the approximate position of the high magnification images in (b) and (e).

© Author(s) 2022

A low magnification image of the sample with low AsH_3 is shown in Fig. 4(c). Small ripples in the morphology appear later during the growth of both samples, about 500 nm into the stack, or 45 repeat units. These ripples are consistent with the formation of step bunches due to the strained-layer growth on a miscut wafer surface[43] and result in a similar lateral thickness modulation to that observed previously. On the sample with low AsH_3 partial pressure, the amount of step bunching gradually worsens, eventually leading to extended defects. However, on the sample with high AsH_3 partial pressure, shown in Fig. 4(f), the material stabilizes, and further elastic relaxation is not observed. A similar type of ripple formation was observed in QW cells with thick barriers, shown in Ref. 8, so it is likely that higher strain in GaAsP encourages this relaxation, as is expected from Ref. 43.

Figure 4(b) shows a magnified image of the sample with low AsH_3. The image is about 500 nm into the layer stack, just prior to the formation of major defects. Lateral thickness variation is observed in both GaInAs and GaAsP, but the variation is greater in GaAsP. It is likely that the thickness variation is accompanied by a concurrent composition variation as a strain-relieving mechanism. The variation worsens throughout the SLS stack, eventually leading to phase separation, plastic relaxation via the formation of dislocations and stacking faults, and the poor final surface morphology observed via AFM [Fig. 4(a)].

Increased arsine partial pressure in the GaInAs layers leads to a stable superlattice, and indirectly leads to reduced variation in the GaAsP layer, as observed in Figs. 4(d)–4(f). Reduced GaInAs lateral thickness modulation is expected with an increase in AsH_3 partial pressure due to decreased group-III adatom mobility[25,47] and is similar to the previously theorized impact of Sb on GaInAs QWs.[44] We suggest that decreased variation in GaInAs also leads to decreased variation in GaAsP due to the impact of the surface on the GaAsP growth. Here, the surface likely contains some composition variation and thus strain variation in addition to thickness variation. It has been shown previously that surface strain variation on a metamorphic surface due to underlying dislocations results in composition variation in subsequent growth.[48] Increased arsine partial pressure reduces composition variation in GaInAs that then leads to less composition variation in GaAsP.

The growth conditions have a clear impact on material quality. Reducing thickness and composition variation by optimizing growth conditions leads to a dramatic improvement in device performance. This device development enables thin-barrier SLS cells with a high fraction of GaInAs in the i-region, which we further explore in the next sections.

OPTICALLY THICK SUPERLATTICE SOLAR CELLS

Using the growth conditions established above, we perform two experiments to increase the optical thickness of the SLS devices. In a first experiment, we systematically vary the GaAsP barrier thickness and composition while stress-balancing to $Ga_{0.895}In_{0.105}As$ with constant composition and thickness. The i-region thickness is kept constant at 2 μm, by varying the number of superlattice repeats within the i-region. The nominal thicknesses and compositions of the barriers in this experiment are 170 Å of $GaAs_{0.9}P_{0.1}$, 100 Å of $GaAs_{0.8}P_{0.2}$, 60 Å of $GaAs_{0.65}P_{0.35}$, 30 Å of $GaAs_{0.5}P_{0.5}$, and 20 Å of GaP. Wafer curvature confirms stress-balancing in all cases.

Figure 5(a) shows the QE as the barrier thickness is varied. As the barrier thickness decreases, the quantum efficiency near the band edge increases due to the increasing amount of total GaInAs within the i-region. The height of the EQE at 800 nm is similar to the baseline performance of thick-barrier devices shown in Fig. 2. The fraction of GaInAs in the i-region increases with thinner GaAsP barriers, as listed in the legend of Fig. 5(a). With a fixed i-region thickness, the total amount of GaInAs increases as the GaAsP barrier is thinned due to the increased number of superlattice repeats. With progressively thinner GaAsP barriers, the total thickness of GaInAs increases from 680 to 1564 nm and the fraction of GaInAs in the SL stack increases from 32% to 80%, respectively. Thus, the absorption beyond the GaAs band edge increases in these thin-barrier devices. Additionally, the Au contact behind the cell acts as an efficient reflector, giving light a second pass through the SL. Thus, in devices with the thinnest barriers, the EQE approaches 100% at 910 nm, implying an efficient collection of carriers generated in GaInAs. Note that these cells can be considered optically thick, but still rely on the use of a back reflector.

In a second experiment shown in Fig. 5(b), the number of repeats, and thus the total thickness of the i-region, is varied in order to further test the potential of optically thick solar cells. In this experiment, the thickness and composition of the barrier were fixed to 60 Å of $GaAs_{0.65}P_{0.35}$ [corresponding to the green curve in Fig. 5(a)] to maintain a high fractional GaInAs content while avoiding high barrier strain and enable the growth of many SL repeats without problematic thickness and composition variation. The number of repeats varies from 100 to 300, which varies the total thickness of the GaInAs from 850 to 2550 nm. GaInAs makes up 57% of the total i-region thickness in all cases, meaning that the thickest i-region in this experiment is almost 4.5 μm thick.

Figure 5(b) shows the EQE as the number of repeats increases. Increasing the number of repeats, and thus increasing the amount of GaInAs, increases the quantum efficiency without any major signs of material quality degradation or limitations of the i-region thickness. The thickest sample has a nearly perfect carrier collection up to 920 nm. Although this sample still benefits from a back reflector, the thickness of the GaInAs is over 2500 nm thick, and so it can be considered optically thick even without a reflector.

Figure 5(c) shows the calculated photocurrent from photons with energy below the GaAs band edge (1.41 eV), using the EQE beyond 880 nm integrated over the AM0 space spectrum, as a function of the total GaInAs thickness in the i-region. Both of the above experiments are shown: using a fixed i-region thickness and increasing the GaInAs by thinning the GaAsP barriers (red line) and using a variable i-region thickness and increasing the GaInAs by increasing the number of SL repeats (blue line). Both routes lead to significant gains in the sub-bandgap current, with both routes achieving equivalent photocurrent for a given total GaInAs thickness.

Figure 6 shows analysis of the JV curves of both experiments shown in Fig. 5, including open-circuit voltage (Voc), fill factor (FF), short-circuit current (Jsc), and efficiency. The bandgap is

© Author(s) 2022

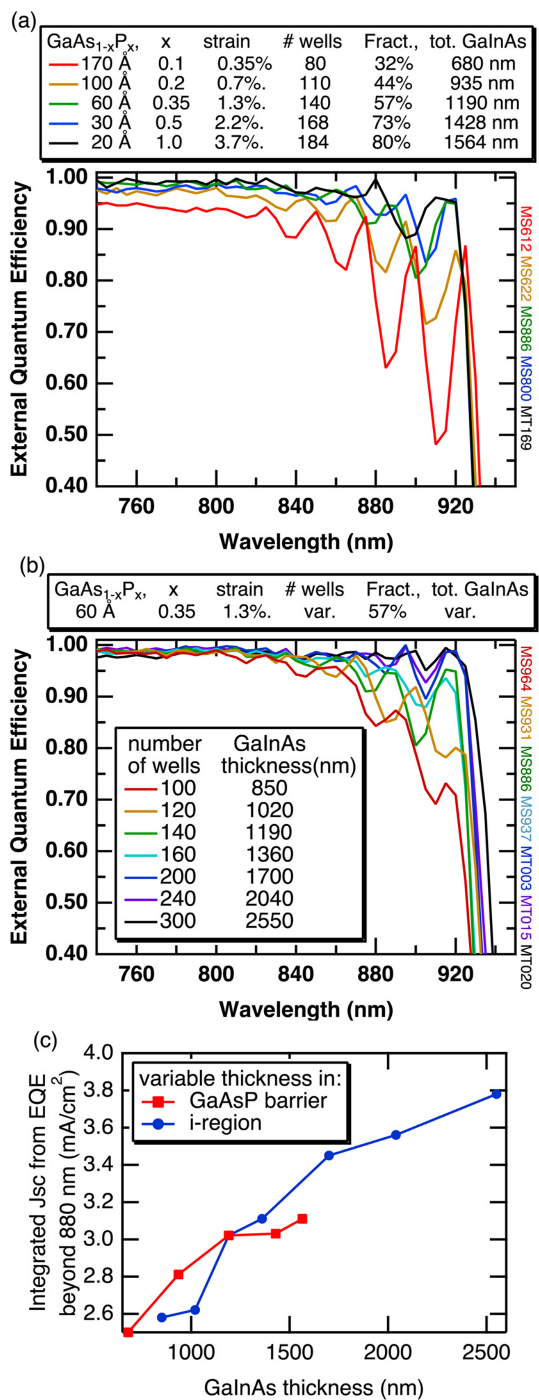

FIG. 5. EQE of stress-balanced GaInAs/GaAsP solar cells with (a) variable GaAsP barrier thickness and composition and fixed GaInAs composition and i-region thickness, (b) fixed GaInAs and GaAsP composition and layer thickness but variable number of repeats and thus i-region thickness. The x-axis is the total GaInAs thickness in the i-region. (c) Integrated Jsc under AM0 from below the GaAs band edge of both approaches to increase photocurrent.

calculated from the EQE using Ref. 49, where "bandgap" here refers to the "absorption edge" of the quantum well or superlattice. To minimize scatter in the data, device analysis is performed on devices all the same size and without anti-reflection coating (ARC).

The increases in Jsc with GaInAs thickness noted in Fig. 5(c) are also observed in Fig. 6 but with greater scatter in the trends. While using JV data from devices without ARC reduces relative error overall, it does lead to higher sensitivity to Fabry–Pérot fringes in the EQE that leads to some scatter in Jsc.

Increasing the total GaInAs thickness by increasing the i-region thickness leads to slow losses in the Voc and FF. Some decrease in both Voc and FF is expected due to an increased depletion region recombination (J_{02}) in devices with wider depletion regions. However, we also note that the bandgap decreases with increasing i-region thickness. There is no change in the deposition parameters, so a decrease in the bandgap is not expected. The

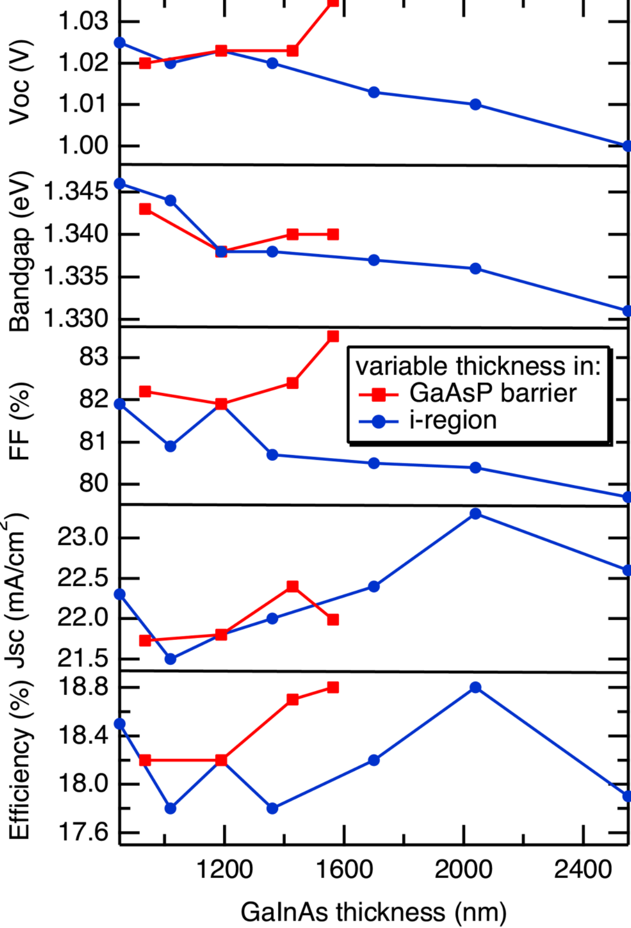

FIG. 6. JV analysis of stress-balanced GaInAs/GaAsP solar cells (without ARC), including open-circuit voltage (Voc), fill factor (FF), short-circuit current (Jsc), and efficiency. All measurements were taken under the AM1.5 global spectrum. The bandgap is calculated from the EQE.

© Author(s) 2022

change in bandgap is 15 meV from 850 to 2550 nm thickness, while the change in Voc is 25 mV, meaning there is ∼10 mV loss in Voc beyond the bandgap change. Although we do not investigate the source of the bandgap reduction, we speculate that the bandgap shift could be related to the slow increase in composition variation as the number of GaInAs/GaAsP repeats increases (Fig. 4). Fortunately, the relatively minor loss indicates that there is no major plastic deformation, which may occur if the composition and thickness variation results in enough strain energy for dislocation formation or other defect generation, such as in Fig. 4(c). The sensitivity of the device to material degradation makes an in-depth modeling of performance difficult. However, all Vocs are excellent. Even the thickest device (4.5 μm i-region, 2.5 μm GaInAs) has a Voc of 1.0 V and a Woc of 0.33 V.

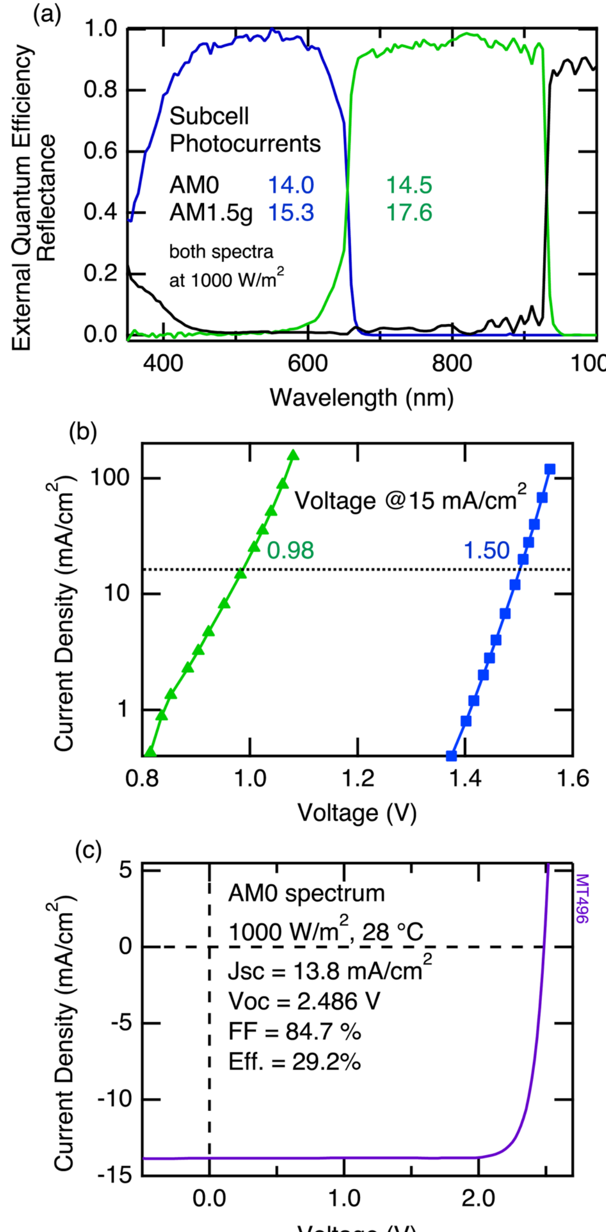

FIG. 7. Two-junction device characterization. (a) EQE and reflectance, and integrated subcell photocurrents under the AM0 and AM1.5 g spectra. (b) Subcell dark JV curves calculated from electroluminescence, and subcell voltages at 15 mA/cm^2. (c) Two-junction JV curve under the 1000 W/cm^2 AM0 spectrum at 28 °C and device metrics.

Increasing the total GaInAs thickness by decreasing the GaAsP barrier thickness and maintaining a constant i-region thickness leads to a different trend in Voc and FF. The Voc and FF do not decrease and may even slightly increase, although data are limited. The expected trends in Voc and FF are complex. Increasing low bandgap material in the intrinsic region should increase depletion region recombination and, thus, increase J0, while raising the bandgap of the high bandgap barriers should have the opposite effect.[50] In addition, the non-radiative recombination may change with the strain and composition in the barrier due to changes in composition modulation or interface quality.[51] With very thin barriers, tunneling transport is expected to reduce escape lifetime (Fig. 1) and have an impact on voltage, which has been observed previously.[52] Here, the thinnest barriers are 2 nm thick, composed of GaP, and are highly strained (3.7%) to the GaAs substrate. Despite the high strain in the barriers, these devices have the highest FF and Voc of both experiments, with 83.5% and 1.035 V, respectively. No change in the series resistance is observed, and a reduced J02 component is observed in the dark JV in cells with GaP barriers. The Woc is 0.31 V, implying an excellent material quality and no negative impact of the GaP barriers.

As shown in Fig. 1, tunneling begins to play a beneficial role in carrier transport in SLS devices with GaAsP barrier thickness < 5 nm.[14,17,21] Thus, the above routes toward increasing total GaInAs thickness (increasing the number of repeats, or decreasing the barrier thickness) in the i-region are not identical. The carrier collection in devices with many wells depends on the nonradiative lifetime in the quantum wells.[33] We note that the quantum efficiency for all samples is near unity above the GaAs bandgap and is near unity below the GaAs bandgap for devices with many quantum wells. Thus, the nonradiative lifetime in the wells is sufficiently long for efficient collection in both routes toward increasing GaInAs thickness. For devices with equivalent total GaInAs thickness in the i-region, samples with very thin barriers should outperform samples with thick barriers if the material quality does not degrade. In this study, the GaP barriers are nominally 2 nm thick and these samples do outperform the devices with thicker barriers and similar total GaInAs, implying a benefit from tunneling without material degradation.

Several performance tradeoffs exist when designing a superlattice solar cell. Because each individual GaInAs layer is thin, many GaInAs/GaAsP superlattice repeats must be incorporated for significant current collection below the GaAs band edge. As the number of repeats increases, the i-region increases and so depletion region recombination increases and performance decreases. However, the material quality may also degrade throughout the superlattice as shown in Fig. 4, leading to performance losses with increasing

© Author(s) 2022

GaInAs/GaAsP repeats. For equivalent total GaInAs thickness, using thin barriers can lead to improved performance. However, we note that the step-bunching that leads to degradation is dependent on the strain.[43] Therefore, the change in the material quality with increasing GaInAs/GaAsP repeats should depend on the strain in the barrier. In this study, we developed superlattice solar cells using $GaAs_{0.65}P_{0.35}$ barriers that would be optically thick without the use of a rear reflector, and solar cells using GaP barriers that are optically thick with the use of a rear reflector. Due to the dependence of the material quality on the barrier strain, it is not known whether optically thick superlattice solar cells can be created using GaP barriers without relying on a rear reflector.

The efficiency of these single solar cells, shown in Fig. 6, has a complex relationship with GaInAs thickness due to the scatter in Jsc as well as the performance tradeoffs described above. For single junction devices, the benefit of sub-GaAs current collection to efficiency is only moderate because the GaAs bandgap is close to optimal. The major benefit for sub-GaAs current collection is to multijunction devices such as GaInP/GaAs two-junction devices where the GaAs bandgap is far from optimal.[53,54]

TWO-JUNCTION STRAIN-BALANCED SUPERLATTICE DEVICES

The GaInAs/GaP SLS solar cell is incorporated into a two-junction device designed for the AM0 space spectrum. The SLS cell is the bottom cell and has a near-identical structure to the sample in Fig. 5(a) with GaP barriers, with 184 GaInAs/GaP repeats and a total GaInAs thickness of 1.56 μm. The top cell is a front-junction, 1-μm-thick, disordered GaInP subcell.[55] Device results are shown in Fig. 7.

The EQE [Fig. 7(a)] of the SLS subcell is near-unity until 920 nm, and the modeled bandgap is 1.34 eV.[49] The top cell bandgap is 1.9 eV. The integrated subcell photocurrents are shown in Fig. 7(a) under the AM0 space spectrum and AM1.5 global spectrum, both using 1000 W/m^2 irradiance. The photocurrents are fairly matched under the AM0 spectrum: 14.0 and 14.5 mA/cm^2 for the top and bottom subcells, respectively, at an irradiance of 1000 W/m^2, and 19.1 and 19.8 mA/cm^2 for the top and bottom cells, respectively, at an irradiance of 1366 W/m^2.

The top and bottom subcell voltages, calculated from the electroluminescence [Fig. 7(b)], are 1.50 and 0.98 V at 15 mA/cm^2, respectively, making the Wocs 0.4 and 0.36 V, respectively. The superlattice Woc is higher in a two-junction device than the single junction device presented in Fig. 6, which is partially due to the lower subcell photocurrent when filtered by the GaInP top cell.

The two-junction device has excellent performance under the AM0 spectrum, as shown by the NREL-certified IV curve in Fig. 7(c). The Voc is 2.486 V, in agreement with the sum of the subcell voltages calculated from electroluminescence. The Jsc from the JV curve, 13.8 mA/cm^2, agrees well with the integrated EQE and is limited by the top cell. The FF is 84.7% and takes advantage of slightly overdriven bottom cell. The overall device efficiency is (29.2 ± 0.4)% under the AM0 spectrum at 1000 W/m^2 and at 28 °C. This beginning-of-life efficiency is significantly higher than the previous two-junction AM0 efficiency of 26.9%, using GaInP and GaAs subcells.[56] Note that devices are often measured under the AM0 spectrum at a higher irradiance of 1366 W/m^2, which would likely increase the efficiency of this new device further. This device, although designed for the AM0 spectrum, has an efficiency of (32.9 ± 0.5)% under the AM1.5 global spectrum, equivalent to a recent record device designed for the global spectrum[8] that used optically thin quantum wells in the bottom cell. The high efficiencies demonstrated in this new device are a result of the more optimal two-junction bandgap combination enabled by the superlattice bottom subcell with very high subcell material quality.

CONCLUSIONS

We have shown the development of optically thick GaInAs/GaAsP strain-balanced superlattice solar cells and demonstrated single junction devices with excellent performance. Thickness and composition variation can develop throughout the GaInAs/GaAsP superlattice and can lead to phase separation and major defects if not controlled. Increasing the arsine partial pressure during the growth of the GaInAs is one successful tactic to limit the material degradation and enable optically thick devices.

Single junction devices with over 2500 nm of GaInAs are demonstrated by incorporating 300 GaInAs/GaAsP repeats, and devices with ~80% fractional GaInAs content in the depletion region are demonstrated by stress-balancing GaInAs with thin layers of GaP. Single junction devices incorporating 2 nm GaP barriers perform better than devices with similar total GaInAs but using thicker barriers, potentially due to the beneficial impact of tunneling on carrier transport in devices with very thin barriers. Near-unity EQE is shown below the GaAs band edge to 920 nm, and superlattice devices with Wocs as low as 0.31 V are demonstrated.

A GaInAs/GaP superlattice subcell was incorporated into a two-junction device along with a 1-μm-thick GaInP top cell, designed to be close to current-matched under the AM0 space spectrum. The two-junction device achieves (29.2 ± 0.4)% efficiency under the AM0 spectrum at 1000 W/m^2 and 28 °C, and (32.9 ± 0.5)% efficiency under the AM1.5 global spectrum at 1000 W/m^2 and 25 °C, despite unbalanced photocurrents under the global spectrum. Subcell Wocs, calculated from electroluminescence and EQE, are 0.4 and 0.36 V for the top subcell and bottom subcell, respectively, highlighting the high material quality in both subcells. The high two-junction efficiency is due to the bandgap combination that is enabled by the high performance superlattice subcell.

ACKNOWLEDGMENTS

The authors kindly thank Michelle Young, Waldo Olavarria, and Alan Kibbler for growth and processing support; Bobby To for AFM; John Geisz for equipment support and valuable conversations; Tao Song, Chuck Mack, and Rafell Williams for measurement support; and Ned Ekins-Daukes and colleagues for valuable conversations and foundational work. This work made use of shared facilities of the UCSB MRSEC (No. NSF DMR 1720256), a member of the Materials Research Facilities Network. This work was authored, in part, by the National Renewable Energy Laboratory, operated by alliance for Sustainable Energy, LLC, for the U.S. Department of Energy (DOE) under Contract No. DE-AC36-08GO28308. Funding was provided by the U.S.

© Author(s) 2022

Department of Energy Office of Energy Efficiency and Renewable Energy Solar Energy Technologies Office, under Award No. 34358. The views expressed in the article do not necessarily represent the views of the DOE or the U.S. Government. The U.S. Government retains and the publisher, by accepting the article for publication, acknowledges that the U.S. Government retains a nonexclusive, paid-up, irrevocable, worldwide license to publish or reproduce the published form of this work, or allow others to do so, for U.S. Government purposes.

AUTHOR DECLARATIONS

Conflicts of Interest

The authors have no conflicts to disclose.

Author Contributions

Ryan M. France: Investigation (lead); Methodology (lead); Visualization (lead); Writing – original draft (lead). **Jennifer Selvidge:** Investigation (equal); Writing – review & editing (equal). **Kunal Mukherjee:** Supervision (equal); Writing – review & editing (equal). **Myles A. Steiner:** Methodology (equal); Supervision (equal); Writing – review & editing (equal).

DATA AVAILABILITY

The data that support the findings of this study are available from the corresponding author upon reasonable request.

REFERENCES

[1]R. M. France, F. Dimroth, T. J. Grassman, and R. R. King, MRS Bull. **41**, 202 (2016).
[2]E. A. Fitzgerald, Mater. Sci. Rep. **7**, 87 (1991).
[3]J. F. Geisz, R. M. France, K. L. Schulte, M. A. Steiner, A. G. Norman, H. L. Guthrey, M. R. Young, T. Song, and T. Moriarty, Nat. Energy **5**, 326 (2020).
[4]J. M. Zahler, A. F. I. Morral, C. G. Ahn, H. A. Atwater, T. J. Watson, M. W. Wanlass, C. Chun, and P. A. Iles, in *IEEE Photovoltaic Specialists Conference*, New Orleans, LA (IEEE, 2002).
[5]U. Gosele and Q. Y. Tong, Ann. Rev. Mater. Sci. **28**, 215 (1998).
[6]F. Dimroth, M. Grave, P. Beutel, U. Fiedler, C. Karcher, T. N. D. Tibbits, E. Oliva, G. Siefer, M. Schachtner, A. Wekkeli, A. W. Bett, R. Krause, M. Piccin, N. Blanc, C. Drazek, E. Guiot, B. Ghyselen, T. Salvetat, A. Tauzin, T. Signamarcheix, A. Dobrich, T. Hannappel, and K. Schwarzburg, Prog. Photovoltaics Res. Appl. **22**, 277 (2014).
[7]I. Sayed and S. M. Bedair, IEEE J. Photovolt. **9**, 402 (2019).
[8]M. A. Steiner, R. M. France, J. Buencuerpo, J. F. Geisz, M. P. Nielsen, A. Pusch, W. J. Olavarria, M. Young, and N. J. Ekins-Daukes, Adv. Energy Mater. **11**, 2002874 (2021).
[9]N. J. Ekins-Daukes, J. M. Barnes, K. W. J. Barnham, J. P. Connolly, M. Mazzer, J. C. Clark, R. Grey, G. Hill, M. A. Pate, and J. S. Roberts, Sol. Energy Mater. Sol. Cells **68**, 71 (2001).
[10]K. W. J. Barnham, I. Ballard, J. P. Connolly, N. J. Ekins-Daukes, B. G. Kluftinger, J. Nelson, and C. Rohr, Phys. E **14**, 27 (2002).
[11]R. J. Chaffin, G. C. Osbourn, L. R. Dawson, and R. M. Biefeld, in *IEEE Photovoltaics Specialists Conference*, Kissimmee, FL (IEEE, 1984), p. 743.
[12]K. W. J. Barnham and G. Duggan, J. Appl. Phys. **67**, 3490 (1990).
[13]M. W. Wanlass and A. E. Blakeslee, in *IEEE Photovoltaic Specialists Conference*, San Diego, CA (IEEE, 1982), p. 584.
[14]R. E. Welser, S. J. Polly, M. Kacharia, A. Fedorenko, A. K. Sood, and S. M. Hubbard, Sci. Rep. **9**, 13955 (2019).
[15]H. Fujii, K. Toprasertpong, Y. Wang, K. Watanabe, M. Sugiyama, and Y. Nakano, Prog. Photovoltaics Res. Appl. **22**, 784 (2014).
[16]J. G. J. Adams, B. C. Brown, I. M. Ballard, J. P. Connolly, N. L. A. Chan, A. Ioannides, W. Elder, P. N. Stavrinou, K. W. J. Barnham, and N. J. Ekins-Daukes, Prog. Photovoltaics Res. Appl. **19**, 865 (2011).
[17]G. K. Bradshaw, C. Z. Carlin, J. P. Samberg, N. A. El-Masry, P. C. Colter, and S. M. Bedair, IEEE J. Photovoltaics **3**, 278 (2013).
[18]J. Nelson, in *Homojunction and Quantum-Well Infrared Detectors*, edited by M. H. Francombe, and J. L. Vossen (Academic Press, 1995), p. 312.
[19]J. Nelson, I. Ballard, K. W. J. Barnham, J. P. Connolly, J. S. Roberts, and M. Pate, J. Appl. Phys. **86**, 5898 (1999).
[20]N. J. Ekins-Daukes, in *Advances in Solar Energy*, edited by D. Y. Goswami (Routledge, London, 2007), Vol. 17, p. 29.
[21]M. Sugiyama, Y. Wang, H. Fujii, H. Sodabanlu, K. Watanabe, and Y. Nakano, J. Phys. D: Appl. Phys. **46**, 024001 (2013).
[22]J. Nelson, M. Paxman, K. W. J. Barnham, J. S. Roberts, and C. Button, IEEE J. Quantum Electron. **29**, 1460 (1993).
[23]P. R. Griffin, J. Barnes, K. W. J. Barnham, G. Haarpainter, M. Mazzer, C. Zanotti-Fregonara, E. Grünbaum, C. Olson, C. Rohr, J. P. R. David, J. S. Roberts, R. Grey, and M. A. Pate, J. Appl. Phys. **80**, 5815 (1996).
[24]N. Y. Jin-Phillipp, F. Phillipp, T. Marschner, and W. Stolz, J. Mater. Sci.: Mater. Electron. **8**, 289 (1997).
[25]R. Bhat, M. A. Koza, D. M. Hwang, K. Kash, C. Caneau, and R. E. Nahory, J. Cryst. Growth **110**, 353 (1991).
[26]J. Tersoff, Y. H. Phang, Z. Y. Zhang, and M. G. Lagally, Phys. Rev. Lett. **75**, 2730 (1995).
[27]J. Tersoff, C. Teichert, and M. G. Lagally, Phys. Rev. Lett. **76**, 1675 (1996).
[28]Y. P. Wang, S. J. Ma, K. Watanabe, M. Sugiyama, and Y. Nakano, J. Cryst. Growth **352**, 194 (2012).
[29]D. C. Johnson, I. Ballard, K. W. J. Barnham, D. B. Bishnell, J. P. Connolly, M. C. Lynch, T. N. D. Tibbits, N. J. Ekins-Daukes, M. Mazzer, R. Airey, G. Hill, and J. S. Roberts, Sol. Energy Mater. Sol. Cells **87**, 169 (2005).
[30]D. B. Bushnell, N. J. Ekins-Daukes, K. W. J. Barnham, J. P. Connolly, J. S. Roberts, G. Hill, R. Airey, and M. Mazzer, Sol. Energy Mater. Sol. Cells **75**, 299 (2003).
[31]R. M. France, P. Espinet-Gonzáles, N. J. Ekins-Daukes, H. Guthrey, M. A. Steiner, and J. F. Geisz, IEEE J. Photovoltaics **8**, 1608 (2018).
[32]R. M. France, J. Buencuerpo, M. Bradsby, J. F. Geisz, Y. Sun, P. Dhingra, M. L. Lee, and M. A. Steiner, J. Appl. Phys. **129**, 173102 (2021).
[33]R. M. France, J. G. Geisz, T. Song, W. Olavarria, M. Young, A. Kibbler, and M. A. Steiner, Joule **6**, 1121 (2022).
[34]M. A. Steiner, R. M. France, J. Buencuerpo, J. Simon, and W. E. McMahon, in *IEEE Photovoltaic Specialists Conference*, Chicago, IL (IEEE, 2019), p. 281.
[35]J. F. Geisz, M. A. Steiner, I. Garcia, S. R. Kurtz, and D. J. Friedman, Appl. Phys. Lett. **103**, 041118 (2013).
[36]A. Duda, S. Ward, and M. Young, "Inverted metamorphic multijunction (IMM) cell processing instructions," Technical Report NREL/TP-5200-54049, 2012; available at https://www.nrel.gov/docs/fy12osti/54049.pdf
[37]M. A. Steiner, J. F. Geisz, T. E. Moriarty, R. M. France, W. E. McMahon, J. M. Olson, S. R. Kurtz, and D. J. Friedman, IEEE J. Photovoltaics **3**, 879 (2013).
[38]U. Rau, Phys. Rev. B **76**, 085303 (2007).
[39]N. J. Ekins-Daukes, K. Kawaguchi, and J. Zhang, Cryst. Growth Des. **2**, 287 (2002).
[40]J. W. Matthews and A. E. Blakeslee, J. Cryst. Growth **27**, 118 (1974).
[41]L. B. Freund, J. Appl. Mech. **54**, 553 (1987).
[42]R. M. France, W. E. McMahon, and H. L. Guthrey, Appl. Phys. Lett. **107**, 151903 (2015).
[43]P. Venezuela, J. Tersoff, J. A. Floro, E. Chason, D. M. Follstaedt, F. Liu, and M. G. Lagally, Nature **397**, 678 (1999).
[44]J. C. Harmand, L. H. Li, G. Partriarche, and L. Travers, Appl. Phys. Lett. **84**, 3981 (2004).
[45]T. Kageyama, T. Miyamoto, M. Ohta, T. Matsuura, Y. Matsui, T. Furuhata, and F. Koyama, J. Appl. Phys. **96**, 44 (2004).
[46]T. Sato, M. Mitsuhara, T. Watanabe, and Y. Kondo, Appl. Phys. Lett. **87**, 211903 (2005).

© Author(s) 2022

[47] R. W. Glew, K. Scarrott, A. T. R. Briggs, A. D. Smith, V. A. Wilkinson, X. Zhou, and M. Silver, J. Cryst. Growth **145**, 764 (1994).
[48] K. Mukherjee, A. G. Norman, A. J. Akey, T. Buonassisi, and E. A. Fitzgerald, J. Appl. Phys. **118**, 115306 (2015).
[49] J. F. Geisz, M. A. Steiner, I. Garcia, R. M. France, W. E. McMahon, C.R. Osterwald, and D. J. Friedman, IEEE J. Photovoltaics **5**, 1827 (2015).
[50] J. P. Connolly, J. Nelson, K. W. J. Barnham, I. Ballard, C. Roberts, J. S. Roberts, and C. T. Foxon, in *IEEE Photovoltaics Specialists Conference*, Anchorage, AK (IEEE, 2000), p. 1304.
[51] A. M. Fox, D. A. B. Miller, G. Livescu, J. E. Cunningham, and W. Y. Jan, IEEE J. Quantum Electron. **27**, 2281 (1991).
[52] K. Toprasertpong, H. Fujii, Y. Wang, K. Watanabe, M. Sugiyama, and Y. Nakano, IEEE J. Photovoltaics **4**, 607 (2014).
[53] D. J. Friedman, Curr. Opin. Solid State Mater. Sci. **14**, 131 (2010).
[54] S. P. Bremner, M. Y. Levy, and C. B. Honsberg, Prog. Photovoltaics Res. Appl. **16**, 225 (2008).
[55] R. M. France, M. Hinojosa, S. P. Ahrenkeil, M. R. Young, S. W. Johnston, H. L. Guthrey, M. A. Steiner, and J. F. Geisz, in *IEEE Photovoltaic Specialists Conference, Virtual* (IEEE, 2021), p. 2522.
[56] T. Takamoto, M. Yamaguchi, S. J. Taylor, M. J. Yang, E. Ikeda, and H. Kurita, Sol. Energy Mater. Sol. Cells **58**, 265 (1999).

© Author(s) 2022